



RESEARCH ARTICLE

10.1002/2016JC011650

Mixing and phytoplankton dynamics in a submarine canyon in the West Antarctic Peninsula

Filipa Carvalho¹, Josh Kohut¹, Matthew J. Oliver², Robert M. Sherrell^{1,3}, and Oscar Schofield¹¹Department of Marine and Coastal Sciences, Rutgers University, New Brunswick, New Jersey, USA, ²College of Earth, Ocean and Environment, University of Delaware, Lewes, Delaware, USA, ³Department of Earth and Planetary Sciences, Rutgers University, Piscataway, New Jersey, USA

Key Points:

- Underwater gliders observe phytoplankton dynamics in Antarctic coastal seas
- Mixed layer depth and water stability as key driver of seasonal phytoplankton blooms
- Contrary to what was initially hypothesized, mUCDW does not seem to play an important role in the phytoplankton spring bloom in the canyon

Correspondence to:

F. Carvalho,
filipa@marine.rutgers.edu

Citation:

Carvalho, F., J. Kohut, M. J. Oliver, R. M. Sherrell, and O. Schofield (2016), Mixing and phytoplankton dynamics in a submarine canyon in the West Antarctic Peninsula, *J. Geophys. Res. Oceans*, 121, 5069–5083, doi:10.1002/2016JC011650.

Received 14 JAN 2016

Accepted 1 JUL 2016

Accepted article online 5 JUL 2016

Published online 24 JUL 2016

Abstract Bathymetric depressions (canyons) exist along the West Antarctic Peninsula shelf and have been linked with increased phytoplankton biomass and sustained penguin colonies. However, the physical mechanisms driving this enhanced biomass are not well understood. Using a Slocum glider data set with over 25,000 water column profiles, we evaluate the relationship between mixed layer depth (MLD, estimated using the depth of maximum buoyancy frequency) and phytoplankton vertical distribution. We use the glider deployments in the Palmer Deep region to examine seasonal and across canyon variability. Throughout the season, the ML becomes warmer and saltier, as a result of vertical mixing and advection. Shallow ML and increased stratification due to sea ice melt are linked to higher chlorophyll concentrations. Deeper mixed layers, resulting from increased wind forcing, show decreased chlorophyll, suggesting the importance of light in regulating phytoplankton productivity. Spatial variations were found in the canyon head region where local physical water column properties were associated with different biological responses, reinforcing the importance of local canyon circulation in regulating phytoplankton distribution in the region. While the mechanism initially hypothesized to produce the observed increases in phytoplankton over the canyons was the intrusion of warm, nutrient enriched modified Upper Circumpolar Deep Water (mUCDW), our analysis suggests that ML dynamics are key to increased primary production over submarine canyons in the WAP.

1. Introduction

The cross-shelf canyon systems in the West Antarctic Peninsula (WAP) are considered biological “hot-spots” because they are associated with penguin chick rearing locations [Erdmann *et al.*, 2011; Fraser and Trivelpiece, 1996]. The association of penguin colonies with deep submarine canyons has led to the hypothesis that phytoplankton productivity is enhanced as a result of water column dynamics in the canyon heads [Schofield *et al.*, 2013]. The presence of the UCDW has been linked to increased phytoplankton productivity [Kavanaugh *et al.*, 2015; Prézelin *et al.*, 2000; Prézelin *et al.*, 2004] which supports a productive regional food web [Schofield *et al.*, 2010], yet the physical mechanisms driving phytoplankton blooms in these canyons are not well understood.

The canyons in the WAP are shelf-incising [Harris and Whiteway, 2011], and often connect the off-shelf region to the coast. Heat transport facilitated by cross-shelf canyons/troughs is enhanced by mixing particularly due to tides [Allen and de Madron, 2009]. Small-scale roughness in canyons can be responsible for much of the internal tidal energy [Kunze *et al.*, 2002], which tends to be enhanced in canyons. Additionally these regions have enhanced internal waves with periods shorter than that of tides, and has been associated with the vertical mixing over the slope and shelf waters [Bruno *et al.*, 2006]. Tides in these canyons also appear to be important for penguin foraging behavior [Oliver *et al.*, 2013] and krill swarms [Bernard and Steinberg, 2013].

These canyons allow UCDW to penetrate across the shelf, providing warmer [Martinson and McKee, 2012; Martinson *et al.*, 2008] and nutrient-enriched water to mix with coastal surface waters [Arrigo *et al.*, 2015; Prézelin *et al.*, 2000; Prézelin *et al.*, 2004]. The presence of these canyons has been connected to locally increased sea surface temperature (SST), reduced sea ice coverage, and increased diatom biomass [Kavanaugh *et al.*, 2015]. Using a model, Allen *et al.* [2001] showed that the formation of an eddy over the head of a canyon trapped passive particles such as phytoplankton and small zooplankton in that location.

© 2016. The Authors.

Journal of Geophysical Research: Oceans published by Wiley Periodicals, Inc. on behalf of American Geophysical Union.

This is an open access article under the terms of the Creative Commons Attribution-NonCommercial-NoDerivs License, which permits use and distribution in any medium, provided the original work is properly cited, the use is non-commercial and no modifications or adaptations are made.

Globally, light and nutrients are key drivers of a bloom, but their relative importance in primary production depends on the region and the role of local stratification. Light is a key factor regulating phytoplankton growth in polar regions, including the WAP. Several studies have linked shallower mixed layer depths (MLD), which increases the overall light available to phytoplankton [Holm-Hansen and Mitchell, 1991; Mitchell and Holm-Hansen, 1991; Moline and Prezelin, 1996; Sakshaug et al., 1991], with increased phytoplankton biomass, especially diatoms [Fragoso and Smith, 2012]. Increased irradiance and vertical stratification have also been positively correlated with increased diatom biomass [Mitchell and Holm-Hansen, 1991; Nelson and Smith, 1991], especially during early spring season [Fragoso and Smith, 2012]. Macronutrients are generally abundant throughout the WAP [Ducklow et al., 2012; Serebrennikova and Fanning, 2004] and although they show marked seasonality [Clarke et al., 2008], in most cases they do not seem to limit phytoplankton growth [Holm-Hansen and Mitchell, 1991]. Micronutrients such as iron do not seem to limit primary production in the coastal waters of the WAP where canyon heads are located either [Annett et al., 2015; Helbling et al., 1991; Martin et al., 1990], but available data are limited.

It is important to understand the link between some of the physical drivers, like stratification and MLD, and phytoplankton dynamics as the higher trophic levels are dependent on primary producers [Schofield et al., 2010]. In this work, we characterize the phytoplankton dynamics in submarine canyons in the WAP using Palmer Deep Canyon (PD) as a focused study area. Here we describe, both temporally and spatially, the phytoplankton spring bloom at PD, using a 6 year Slocum glider dataset. The high spatial and temporal resolution sampling provides a detailed analysis of the phytoplankton and physical dynamics at the head of a submarine canyon in the WAP. While the mechanism initially hypothesized to produce the observed increases in phytoplankton over the canyons was the intrusion of warm, nutrient-enriched mUCDW [Prézelin et al., 2000; Prézelin et al., 2004; Schofield et al., 2013], our analysis suggests that ML dynamics are key to increased primary production over submarine canyons in the WAP.

2. Materials and Methods

2.1. Slocum Gliders

Slocum electric gliders are a robust tool to map in high-resolution the upper water column properties in different environments [Schofield et al., 2007] including polar regions [Kohut et al., 2013; Oliver et al., 2013; Schofield et al., 2013]. These 1.5 m torpedo-shaped buoyancy-driven autonomous underwater vehicles provide high-resolution surveys of the physical and bio-optical properties of the water column [Schofield et al., 2007]. Data were collected using both shallow (100 m depth range) and deep (1000 m) gliders. However, only data above 100 m were considered for this analysis as we are focusing on processes within the euphotic zone. All gliders were equipped with a Seabird Conductivity-Temperature-Depth (CTD) sensor and WET Labs Inc. Environmental Characterization Optics (ECO) pucks, which measured chlorophyll-*a* fluorescence, and optical backscatter at 470, 532, 660, and 700 nm. Glider based conductivity, temperature, and depth measurements were compared with a calibrated ship CTD sensor on deployment and recovery to ensure data quality, as well as with a calibrated laboratory CTD prior to deployment. Glider profiles were binned into 1 m bins and assigned a midpoint latitude and longitude.

2.2. Sampling Overview

Our analysis includes all available concurrent glider physical and biological profiles in the WAP region (Figure 1) where bathymetric depressions have been linked to deep-water intrusion onto the shelf, with a focus on the dynamics at PD. Overall, the data include 26,455 profiles, 265 deployment days, and 3,937 km flown. For comparison purposes, the WAP-shelf analysis excluded all the points in PD region (purple rectangle in Figure 1).

The deployments on the shelf along the WAP were part of the NSF Palmer-Long-Term Ecological Research Project (PAL-LTER) [Ducklow et al., 2007] effort, with the goal of understanding changes (1) in the entire WAP ecosystem with 26 deployments conducted throughout the peninsula from Anvers Island to Charcot Island (-64° to -69° latitude) and (2) with a focus on the PD region where Palmer Station is located. In the PD region (Figure 1, right), data were collected during six field seasons (2010–2015) over the austral summer as part of the NSF PAL-LTER and one field season (2014–2015) as part of the NSF CONVERGE Project [Kohut et al., 2014]. Gliders were deployed from Palmer Station (Anvers Island) with the goal of characterizing PD, focusing on the head of the canyon.

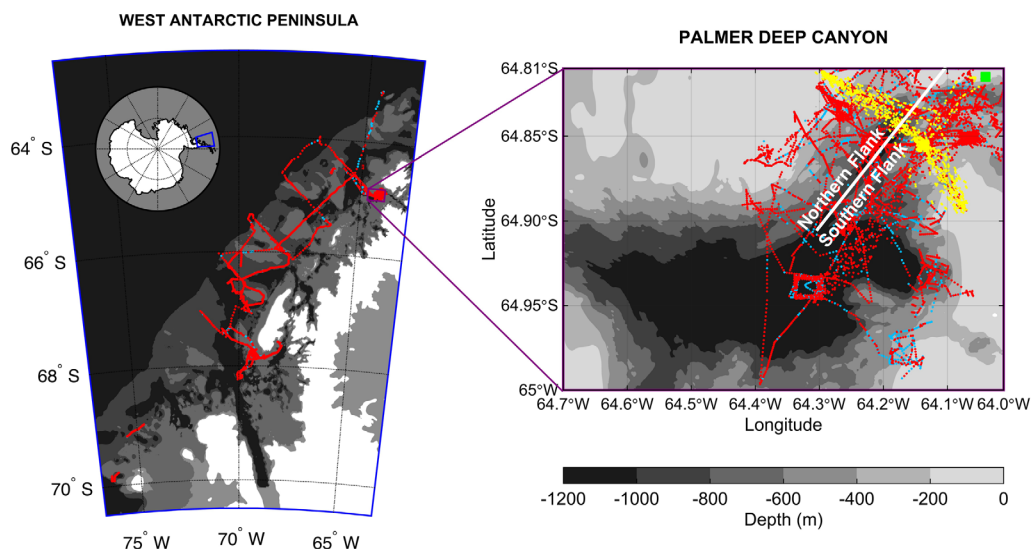


Figure 1. Bathymetry maps overlaid with location of the glider profiles (red – MLD Quality index (QI) > 0.5; blue dots, remaining profiles where MLD was not determined and therefore not included in the analysis, i.e., QI < 0.5) for the regions, (left) WAP and (right) PD. Cross-canyon transects highlighted in yellow from the 2015 mission (gliders ru05 and ud134). White line separates the head of the canyon into northern and southern flanks. Green square indicates location of Station E where dissolved iron data were collected.

PD (Figure 1, right), a cross-shelf canyon bathymetrically similar to others in the WAP, is associated with large penguin colonies [Fraser and Trivelpiece, 1996; Schofield *et al.*, 2013]. PD extends approximately 22 km in length and 10 km across with a maximum depth of 1420 m. Over the head of the canyon, there is evidence of increased primary production [Kavanaugh *et al.*, 2015] and localized penguin foraging [Oliver *et al.*, 2013]. Our study will describe glider data collected over varying spatial scales from the WAP shelf, to PD, and, at the smallest scale, the head of PD.

2.3. Mixed Layer Depth Estimation

For each profile, MLD was determined by finding the depth of the maximum water column buoyancy frequency, $\max(N^2)$. A quality index (Equation 1) following Lorbacher *et al.* [2006] was used to quantify the uncertainty in the MLD estimate, and to filter out profiles where MLD was not resolved. Using

$$QI = 1 - \frac{\text{rmsd}(\rho_k - \bar{\rho})|_{(H_1, H_{MLD})}}{\text{rmsd}(\rho_k - \bar{\rho})|_{(H_1, 1.5 \times H_{MLD})}} \quad (1)$$

where ρ_k is the density at a given depth (k) and $\text{rmsd}()$ denotes the standard deviation of from the vertical mean $\bar{\rho}$ from H_1 , the first layer near the surface, to the MLD or $1.5 \times \text{MLD}$. This index evaluates the quality of the MLD computation, where MLD was determined with certainty ($QI > 0.8$), determined but with some uncertainty ($0.5 < QI < 0.8$) or not determined ($QI < 0.5$). This index does not take into account the strength of stratification, rather it indicates that there is a homogeneous layer present and the MLD calculated is close to the lower boundary of that vertically uniform surface layer. Higher QI are observed during summer and fall, where sharp gradients at the base of the seasonal mixed layer are present [Lorbacher *et al.*, 2006].

MLD criteria were tested and matched against the chlorophyll fluorescence data to evaluate whether the MLD definition chosen was capturing the biological observations (Figure 2). ML-averaged temperature and salinity were calculated by averaging all 1-m binned data points from the surface to the base of the ML.

2.4. Optical Measurements

2.4.1. ML-Averaged and Integrated Chlorophyll

Chlorophyll- a (chl- a) fluorescence, as measured by the glider ECO pucks, is our indicator of phytoplankton biomass. Discrete in situ water samples were collected from eight depths (0, 5, 10, 20, 35, 50, and 60 m) from CTD casts during each glider deployment and recovery. Water samples were filtered onto 25 mm Whatman GF/F filters and extracted using 90% acetone. Chl- a concentration was then measured using a fluorometer and compared to its correspondent glider profiles. QA/QC methods were applied to the data to ensure data quality. Concurrent measurements of optical backscatter and chl- a fluorescence were used to

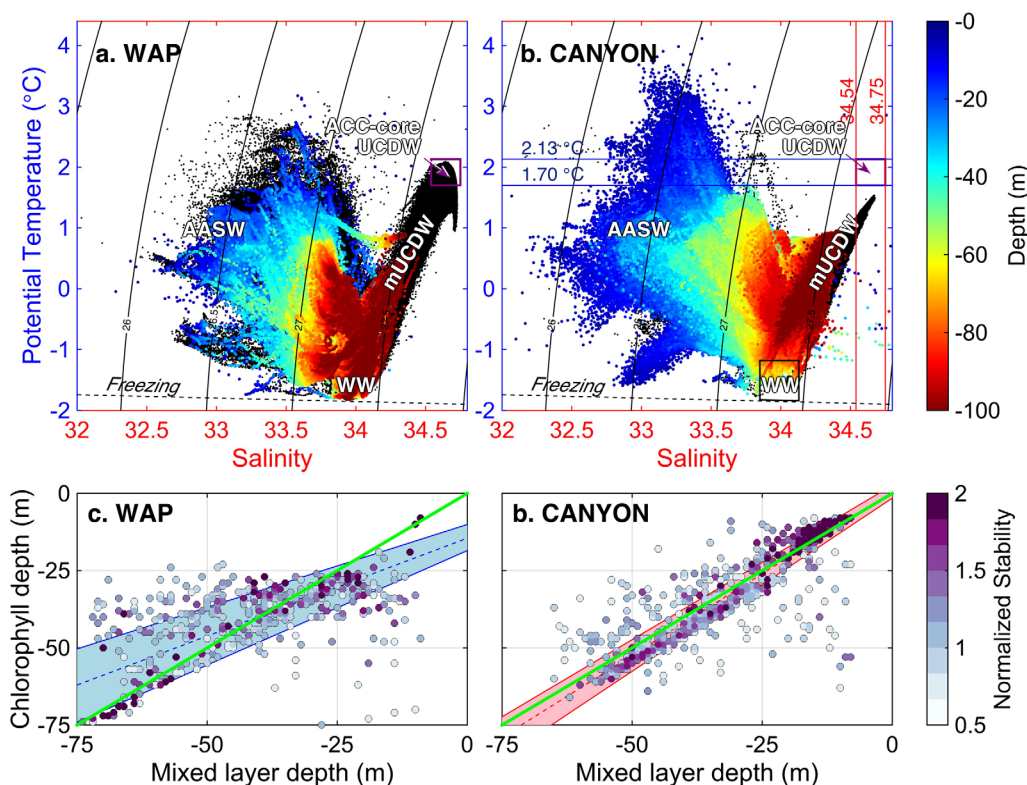


Figure 2. (top row) θ -S for the two areas shown in Figure 1: (a, c) WAP, and (b, d) Palmer Deep Canyon. All data collected below 100 m are plotted in black. Color indicates depth of the water column measurement (upper 100 m of the water column). Primary water masses sampled are indicated and labeled (WW = Winter Water; AASW = Antarctic (summer) Surface Water; mUCDW = modified Upper Circumpolar Deep Water; and the regional ACC-core UCDW). (bottom row) Scatter plots comparing depth of the mixed layer (MLD) with the depth of the lower boundary of the chlorophyll profile for all glider profiles with Quality Index (QI) over 0.5. Shaded region represents 95% confidence intervals (CI) for each region. Trend lines are shown for each area and each quality index. Line 1:1 shown in green. A quality index of 0.5 was also applied to chlorophyll (QI_{chl}) profiles and only profiles with $QI_{chl} > 0.5$ are shown above. Color of the dots represents normalized stability, i.e., the stability frequency at the depth of the ML divided by the median stability of that region.

correct for light-dependent effects. Given the high linear correlation found between backscatter and chlorophyll-*a* fluorescence (R^2 between 0.76 and 0.95 for all deployments), a correction was applied to the latter to account for nonphotochemical quenching [Behrenfeld *et al.*, 2005]. Linear regressions were calculated by deployment using all the measurements taken between 20 and 40 m, below the light influenced chl-*a* values and above the possible sedimentary (deep) sources of backscatter. Slope and intercept were calculated and used to correct chlorophyll from the surface to the chlorophyll maximum in each profile. No chlorophyll maxima were found shallower than 15 m.

Integrated and averaged chlorophyll from our defined MLD to the surface were determined using the trapezoid method. Chl-*a* concentration was calculated for each 1 m bin and a cumulative value from the surface down to the MLD was calculated to determine the ML-integrated chlorophyll. The ML-averaged chlorophyll was determined by dividing the ML-integrated chlorophyll by the depth of the mixed layer.

2.4.2. Chlorophyll Depth

A model-2 regression was used to compare the MLD with the lower boundary of the surface chlorophyll fluorescence layer. Following a method adapted from the maximum angle principle [Chu and Fan, 2011], the depth of lower boundary of chlorophyll was estimated (referred to as chlorophyll depth in Figure 2). Here we apply the same principle using the maximum angle, as we are interested in calculating the depth at which the chlorophyll profile starts decreasing. Using a vector of $n = 7$ data points, the depth of the max ($\tan\theta$) of the chlorophyll profile was determined and used as the chlorophyll depth.

2.5. Climatology

One of the main goals of this study is to characterize the physical setting and to map the seasonal phytoplankton dynamics at the head of the PD by taking advantage of the high spatial and temporal glider

coverage. Using a 6 year data set of glider deployments (13,972 profiles after all filters applied), MLDs were calculated for each individual profile and daily MLD averages were calculated for temperature, salinity and chlorophyll by averaging all the values between the surface and the base of the MLD.

Wind and Photosynthetic Available Radiation (PAR) data were collected from an automated weather station (AWS) at Palmer Station, on Anvers Island. Daily averages were calculated using 2 min data.

2.6. Seawater Iron Methods

Surface water was collected at LTER Station E (6.5 km NE of the head of PD), at eight time points between 5 January and 9 March 2015. Samples were cleanly collected in duplicate from a Zodiac inflatable boat using all-polypropylene syringes and filtered directly into 60 mL LDPE bottles (Nalge®) using 25mm Acrodisc (Pall®) 0.45 μm pore size syringe filters, within minutes of sample collection. The resulting samples were stored at 4°C until arrival at Rutgers University, where they were acidified to pH~2.0 with ultrapure HCl (Fisher Optima®, concentration in seawater 0.012 M). The mean of the duplicates is reported if they agree within 15% (difference about the mean), otherwise the lower of the two values is reported.

Seawater samples were prepared for analysis of dissolved Fe and other trace metals at Rutgers University using the commercially available version of an automated preconcentration and matrix elimination system (SeaFAST pico®, ESI, Omaha, NB) which operates on the same principle as reported in Lagerström *et al.* [2013], and employs the method of isotope dilution, but collects eluates offline rather than directly analyzing online.

The eluate solutions, 25-fold concentrates of the trace metals in the sample but with greatly reduced major ion concentrations, were analyzed in medium resolution on a Thermo Element-1 HR-ICP-MS. Determined process blanks for Fe typically averaged 0.040 nM and precision was 1–3% standard deviation about the mean. Accuracy was verified by repeated analysis of reference seawater materials (SAFE S and D2, GEOTRACES S, and D), which showed agreement within one standard deviation of the consensus values.

2.7. Cross-Canyon Analysis

To better understand the across canyon spatial variability in MLD and chlorophyll, a 1 month long glider mission was designed with a repeated transect (yellow, Figure 1) that crossed the head of the canyon perpendicularly to its deep channel axis (64°48.7'S and 64°17.9'W to 64°53.7'S and 64°4.2'W, corresponding to the northern and southernmost extreme of the transect, respectively). Gliders used for this temporal/spatial study were both shallow gliders (ru05 and ud134) rated to 100 m. The first glider (ud134) was deployed 6 January 2015 and performed six full transects before ru05 took over its mission of surveying the head of the canyon. The second glider was recovered, brought back to Palmer Station, and redeployed twice more during its mission to replace batteries and resume the cross-canyon mission. Final recovery took place on 8 February 2015. Gliders repeated transects across the head of the canyon 39 times throughout their missions, taking an average of 16 h to complete each cross section. The orientation of PD was used to divide (Figure 1, white line) the head of the canyon into two regions, the northern and the southern flanks.

3. Results

3.1. Physical Properties Around the Palmer Deep Canyon

Gliders were able to map many of the key water masses during the austral summer in the WAP shelf and PD region (top plots of Figure 2). The glider profiles over six field seasons identified the Antarctic Surface Water (AASW), Winter Water (WW), and modified Upper Circumpolar Deep Water (mUCDW). The core-UCDW seen immediately offshore of the WAP shelf ($1.7 \leq T \leq 2.13$; $34.54 \leq S \leq 34.7$, following Martinson *et al.* [2008]) was not present in the canyon; instead the canyon was characterized by a modified colder and fresher mUCDW water mass. This mUCDW extended to depths below 100 m. A second water mass present in PD was the WW (or T_{min} , minimum temperature), defined by $T \leq -1.2^\circ\text{C}$ and $33.85 \leq S \leq 34.13$. The WW represents the remnants of the mixed-layer water from the previous winter [Martinson *et al.*, 2008] and was found over a range of depths. Above the WW was the AASW (seen in the blue colors of Figure 2). In the canyon, AASW showed a wider range of temperature, salinity, and depth. In both the WAP and PD, this water mass was freshest of all the water masses present. The main differences between the PD and the WAP shelf (PD profiles were excluded from the latter) were the absence of core-UCDW and fresh surface waters at PD. WW was found at greater depths in the WAP compared to the canyon.

We evaluated the relationship between the MLD and chlorophyll depth with a model-2 linear regression (Figures 2c and 2d). In the canyon, the MLD-chlorophyll relationship was close to a 1:1 line with 95% confidence levels with the tightest regression associated with the profiles with the highest stability. Generally the PD had shallower MLD than the WAP. Although more profiles in the WAP fell away from the 1:1 line, there were no significant differences (with a 95% CI) from that line for MLDs below 23 m.

3.2. Coupled Dynamics at Palmer Deep Canyon

3.2.1. Seasonal Climatology of MLD and Chlorophyll

A seasonal climatological analysis of the MLD properties (Figure 3) was conducted by averaging the data between the surface and the corresponding ML for temperature, salinity, and chlorophyll-*a* fluorescence. Generally, MLD shoaled in December, reaching its shallowest depth ($\overline{MLD} = -11 \pm 0.76$ m) in the beginning of January. MLD remained fairly constant (above 20 m) throughout most of January, then started to deepen at the end of this month. The ML in January was generally fresher and colder and as it deepened it became warmer and saltier. Wind speed was fairly constant and low until late January. From then, there was increasing wind speed until the end of the growing season. The summer MLD reached its maximum depth ($\overline{MLD} = -52 \pm 0.66$ m) during the first week of February and then started shoaling again in early March. Both the temperature (Figure 3a) and salinity (Figure 3c) showed a very clear temporal signal. Secondary shoaling of the ML in mid-February was accompanied by a freshening and slight cooling of the ML. The ML-averaged chlorophyll (Figure 3b) was highest when MLD was shallowest, i.e., throughout January. Going into February, when MLD was deepest, chlorophyll concentrations were low. ML-averaged chlorophyll showed a direct relationship with MLD ($y = 0.136x + 7.03$; $r^2 = 0.42$; $p < 0.0002$), with higher chl-*a* when MLD is shallow and lower chl-*a* when deeper. An increase in chlorophyll was observed when MLD shoaled again later in the season. Surface dissolved iron (Fe) concentrations (Figure 3d) at a station 6.5 km from the

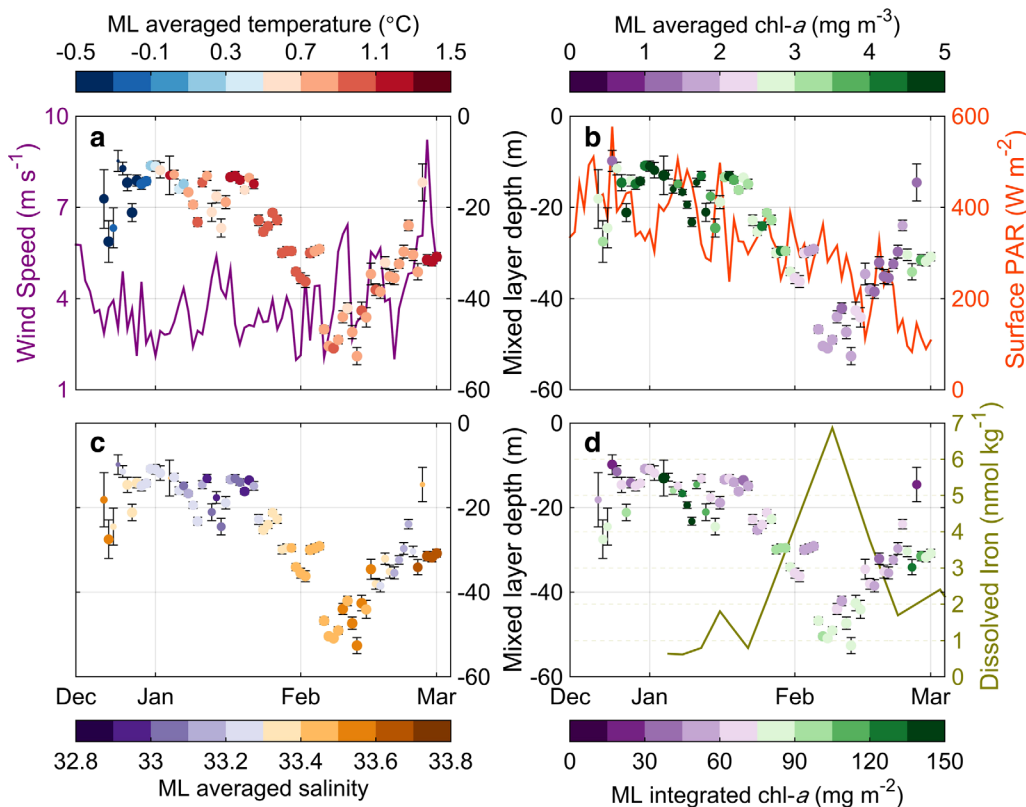


Figure 3. Mixed Layer Depth (MLD) in the Palmer Deep region showing evolution on MLD throughout the spring/summer season. Color denotes ML-averaged: (a) temperature, (b) chlorophyll, (c) salinity, and (d) ML-integrated chlorophyll. Marker size represents the standard error of the variable in color (larger marker represents lower standard error, and vice-versa). Standard error of depth MLD is shown in the vertical bars. Averages were calculated using 13,972 individual glider profiles collected during 2010–2015 deployments. Daily averages of wind and surface PAR are shown in Figures 3a and 3b, respectively. Surface iron measurements at Station E are shown in Figure 3d from 2014–2015 season.

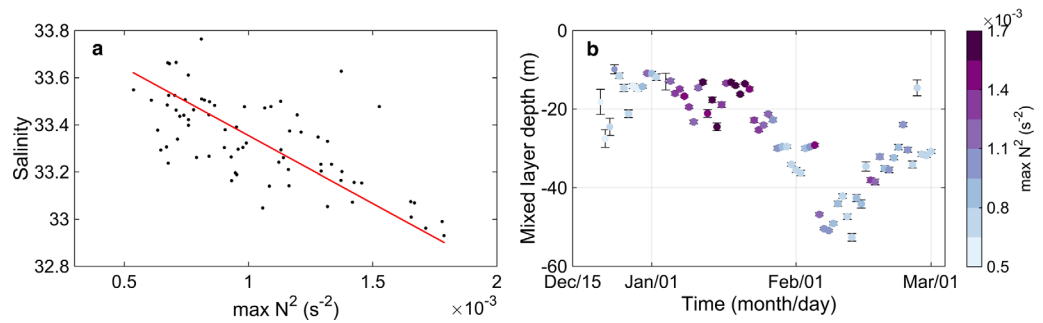


Figure 4. Water stability in the Palmer Deep region using daily averages: (a) salinity and maximum of stability frequency ($\max N^2$); (b) seasonal climatology of MLD with $\max(N^2)$. Averages were calculated using 13,972 individual glider profiles collected during 2010–2015 deployments.

canyon head, exhibited an inverse relationship with chlorophyll, reaching maximum values when MLD was deepest. Throughout the season, Fe concentrations at this station never fell below 0.6 nmol kg^{-1} .

The strength of water column stratification at the depth of the ML ($\max N^2$) was seen to vary through the season (Figure 4). In January, when chlorophyll concentrations were high, the water column was more stable (Figure 4b) and over the season the water column stability decreased. Stability was inversely correlated with salinity ($R^2 = -0.77, p < 0.0001$), with higher stability associated with shallower MLD and lower salinities (Figure 4a) suggesting the importance of sea ice melt and potentially glacial melt in phytoplankton primary productivity.

3.2.2. Cross-Canyon Variability

Four glider deployments, conducted over 1 month, collected high-resolution data across the head of the canyon in PD with the goal of understanding the dynamics of the water masses in the canyon over the summer season. The mission characterized the spatial variability between the northern and southern regions of PD (Figure 1). A temporal and spatial analysis of the θ -S plot is shown in Figure 5. The AASW, represented by the shallowest depths (blue), was cold and fresh in the beginning of January. As the month progressed, surface water became warmer and saltier. Winter water ($T < -1.2^\circ\text{C}$), was present in the beginning of January and was found in deeper waters as time progressed. Deeper water (reds) was warmer and saltier in the beginning of January. The AASW was warmer at the beginning of February (Figure 5, last column).

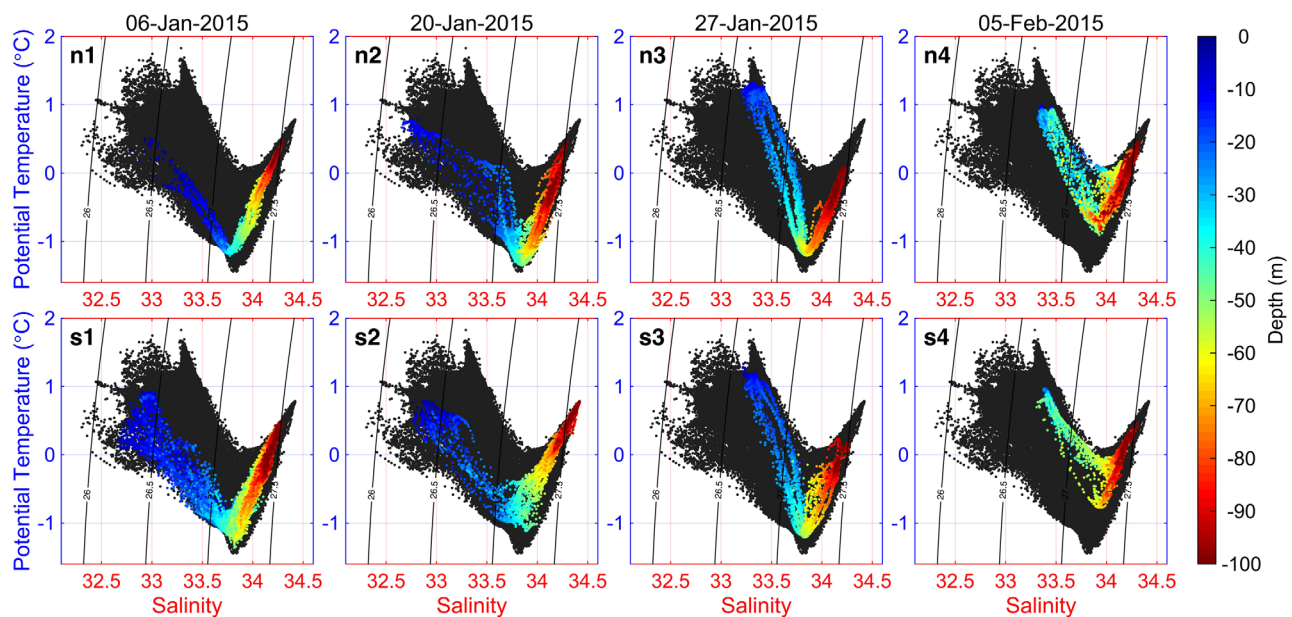


Figure 5. θ -S scatter plots from ru05/ud134 gliders, comparing the water masses of Northern (N, top) and Southern (S, bottom) flanks of the head of the Palmer Deep canyon through time (plots left to right). Black dots represent all glider measurements (both areas) for the entire deployment. Color denotes depth of the water column measurement.

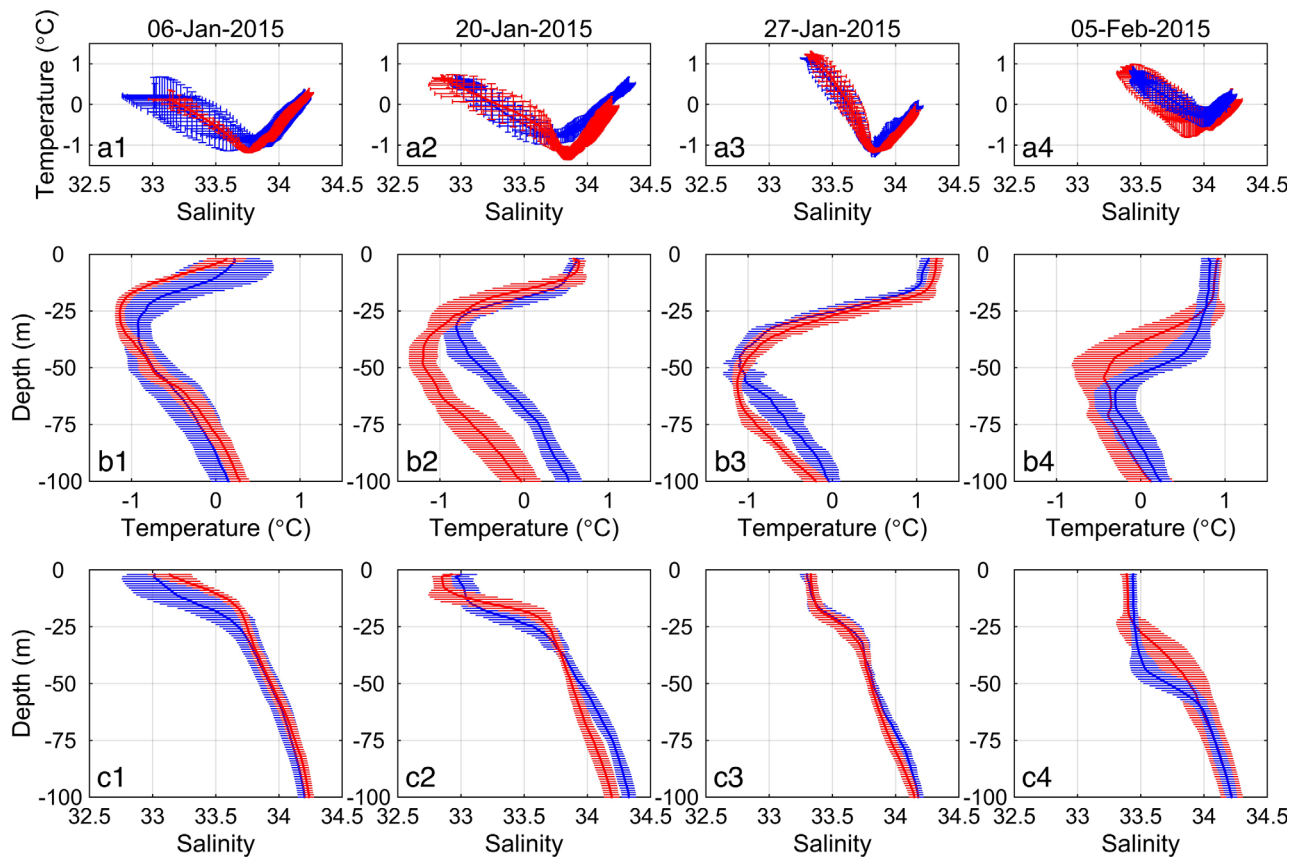


Figure 6. Decomposition of the θ - S diagrams from Figure 5, for Northern (red) and Southern (blue) flanks of the head of the Palmer Deep canyon: (a1–a4) average θ - S diagram with average (center points) and standard deviation (horizontal bars for salinity; vertical bars for temperature), (b1–b4) average temperature profile, (c1–c4) average salinity profile, with standard deviation (shaded area), per depth for each time point.

Given the importance of ML structure in driving the chlorophyll, the θ - S plots in Figure 5 were decomposed into average depth profiles (Figure 6). The average temperature (b plots, middle row) and salinity (c plots, bottom row) depth profiles for each time point, were calculated and then compared between the two regions (blue and red) at the head of the PD canyon. The top row in Figure 6 is for the average distribution and respective standard deviation for the temperature and salinity for each depth and different time periods over the month. The southern region (blue, Figure 6a1) showed overall a wider range in temperature and salinity in the beginning of January. This increased variance was especially marked in AASW, which was characterized by lower salinities. This trend reversed over the month with the northern region of the canyon (red) showing a wider variance in surface water properties (both temperature and salinity). Observed differences were more influenced by temperature (Figures 6b1–6b4) than by salinity (Figures 6c1–6c4). Although surface temperatures were similar between regions, below the MLD, the northern region (red) had consistently lower temperatures (Figures 6b1–6b4) compared to the southern region. Differences of over 0.5°C , sometimes almost up to 1°C , were found at depth on 20 January (Figure 6b2). Both areas showed similar salinity profiles in January. The only salinity differences found were in February and were mostly due to deeper MLDs in the southern region.

The ML-averaged and integrated chlorophyll were calculated for each profile and plotted against its corresponding MLD (Figure 7). Here we define the end of the bloom (21/22 January) by evaluating the evolution of individual profiles of chlorophyll and the change of the trends between MLD and chl- a through time. This date separated two time periods, one during bloom conditions (blue, from 5 to 21 January) and the second during postbloom conditions (red, from 22 January to 9 February). Bloom conditions were characterized by a clear progression from a moderately shallow (30 m) and highly productive MLD (dark blue) to an even shallower (8 m) and less productive ML (light blue). Both ML-integrated (Figure 7a) and averaged chlorophyll (Figure 7b) showed similar trends. While ML-averaged chlorophyll decreased with the deepening of

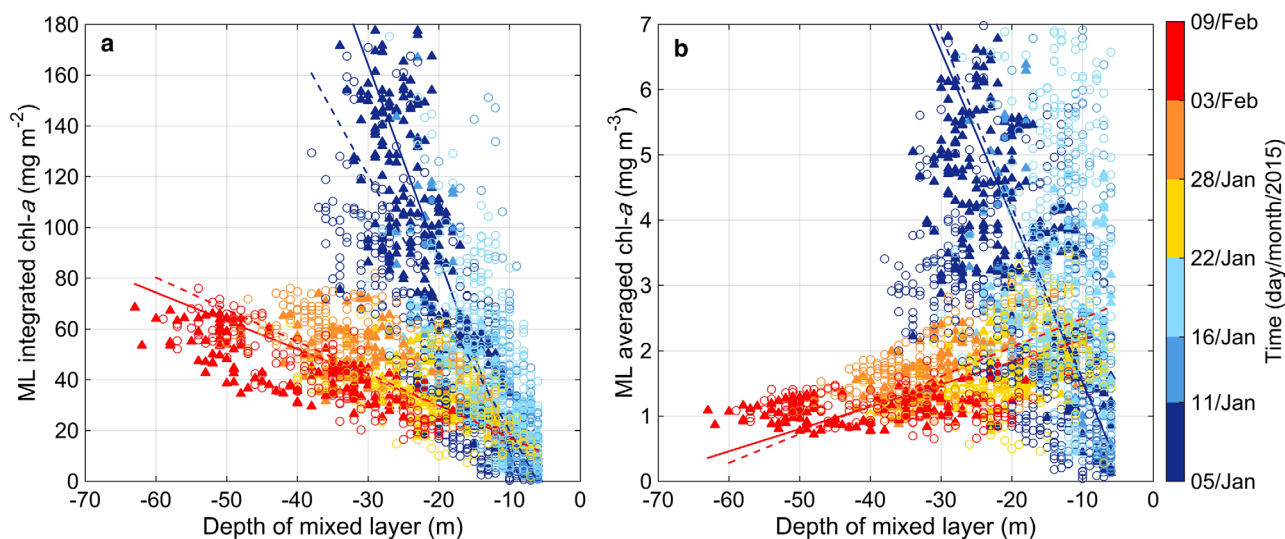


Figure 7. Relationship between the depth of the mixed layer (defined by the maximum water column buoyancy frequency, N^2) and: (a) ML-integrated or (b) ML-averaged chlorophyll concentrations. Comparison between the northern (filled marker, solid line) and southern (open marker, dashed line) flanks. The colors indicate time. Lines represent the trends seen between 6 January to 21 January (blue) and 22 January to 9 February (red).

the ML and consequent ending of the bloom, ML-integrated chlorophyll increased during this postbloom condition (Figures 7 and 9e). When comparing the two regions (northern-solid line; southern-dashed line), few differences were found.

Sustained cross-canyon sampling in 2015 allowed for an analysis for the spatial differences within the canyon. The time-averaged transect (6–28 January 2015) for temperature and salinity is shown in Figures 8a and 8b. While the warm surface layer appears uniform in both regions, a thicker and colder layer (light blue), with a tongue of colder ($T < -1^\circ\text{C}$; dark blue) water at mid depths of 45–70 m was evident in the northern region. The southern region showed warmer and saltier water at depths below the colder layer. A fresher layer was evident in the surface few meters in the northern region. The bottom plot of Figure 8 shows a time-averaged mixed layer depth (blue dotted line) and upper 100 m integrated chlorophyll (solid green line) for each 1 km along the transect line. Northern region was characterized by shallower MLD

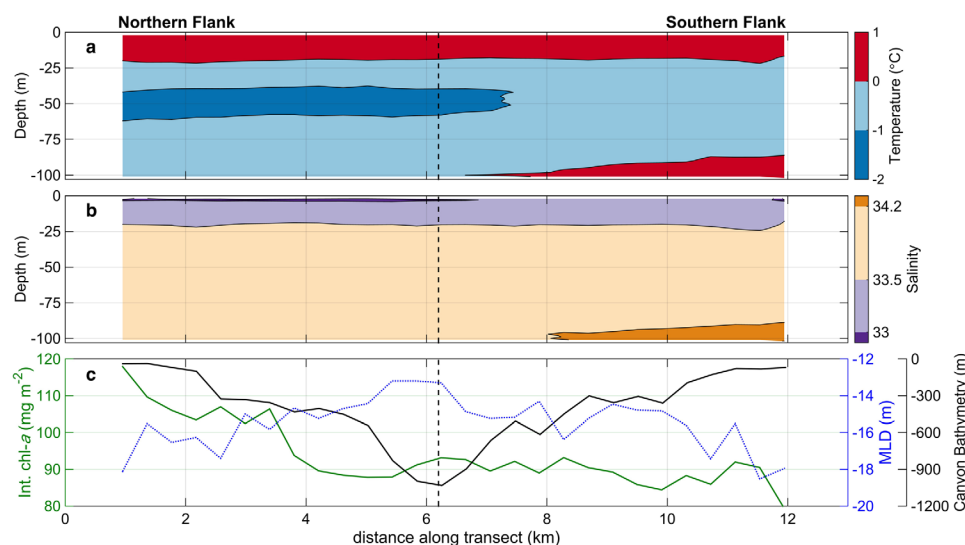


Figure 8. Time-averaged transect (6 January to 28 January 2015). Northern and Southern regions are separated by the dashed vertical line at km 6.2 in the along-track distance. Variables plotted are time-averaged transect of: (a) temperature, where warm layer at the surface represents AASW, dark blue denotes WW, bottom layer in red indicates possibly mUCDW intrusion; (b) salinity and (c) mixed layer depth (MLD; blue-dotted line) with integrated chlorophyll (upper 100 m; green solid line) and canyon bathymetry (black solid line).

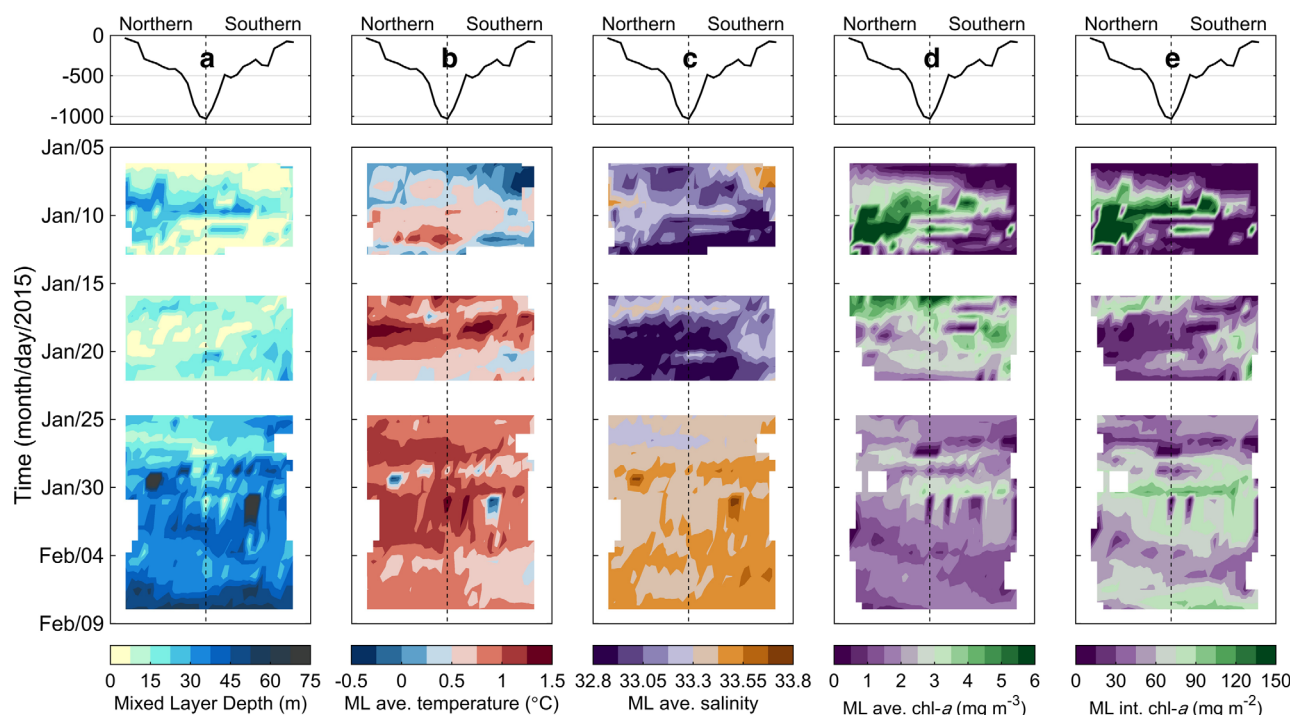


Figure 9. (top) Bathymetry of the cross-canyon transect performed by ru05 (yellow, Figure 1). (bottom) Hovmöller diagram of the temporal evolution of each transect by ru05 regarding: (a) mixed layer depth, (b–d) ML-averaged (b) temperature, (c) salinity, (d) chlorophyll, and (e) ML-integrated chlorophyll. Dashed line separates northern and southern flanks of the head of the Palmer Deep canyon.

and increased integrated chlorophyll in the upper 100 m of the water column while the southern region showed overall deeper MLD and slightly lower integrated chlorophyll concentrations.

A repeated glider section across the head of the canyon captured the temporal and spatial variability of the phytoplankton (Figure 9). Each glider cross section was interpolated through space and time with a resolution of 500 m and 16 h, respectively. Temporal gaps in Figure 9 correspond to glider recovery and redeployment after battery exchange. The top plot shows bathymetry of the two regions (northern and southern) being fairly symmetrical, going from deeper (~ 1000 m) depths at the center to shallower depths (~ 100 m) when moving away from the deep trough.

Again, the temporal signal is the most evident across all five plots. Early in January, the MLD was shallow, colder, and fresher. This period was also characterized by increased chlorophyll (both ML-integrated and averaged chlorophyll). As January progressed, the MLD (Figure 9a) deepened, accompanied by warming (Figure 9b) and increased salinity (Figure 9c) in the upper ML with a decrease in the chlorophyll concentration (Figures 9d and 9e). An increase in ML-integrated chlorophyll (Figure 9e) late in the mission is also present in the climatology (Figure 3).

The magnitude of the spatial variability was less than the temporal variability observed over the entire summer season, yet differences were observed, particularly in the physical properties of the water. The MLD was overall shallower in the northern region. This is especially true for the second and fourth deployments. Warmer temperatures and lower salinities also characterized this region. This pattern was also clear when looking at the homogeneous surface ML later in the season (Figures 6b4 and 6c4).

4. Discussion

The WAP ecosystem is characterized by high interannual phytoplankton variability [Smith *et al.*, 2008], with chlorophyll-*a* showing a wide range in both time and space [Moline *et al.*, 1997; Montes-Hugo *et al.*, 2008; Smith *et al.*, 1998]. Chlorophyll concentrations are highest near shore with a decreasing gradient moving offshore [Vernet *et al.*, 2008]. The canyons are known hotspots for penguin foraging [Kahl *et al.*, 2010; Oliver *et al.*, 2012; Schofield *et al.*, 2013] with increased chlorophyll compared to coastal regions with shallow

bathymetry [Kavanaugh *et al.*, 2015]. While previous studies have focused on the primary productivity over the entire WAP [Moline and Prezelin, 1996; Montes-Hugo *et al.*, 2010; Prézelin *et al.*, 2004], the high-resolution sampling capabilities introduced with gliders, allowed us to conduct a detailed analysis of the canyon primary production focusing on the physical forcing of the increased production observed over submarine canyons.

4.1. The Seasonal Cycle at Palmer Deep Canyon

4.1.1. Primary Water Masses

A fundamental question regarding phytoplankton dynamics in the region [Schofield *et al.*, 2013] involves the supply of heat and nutrients from the warm, deep water (UCDW) found at depth off the shelf. Canyons provide a conduit for this water to move across the shelf [Martinson *et al.*, 2008]. No direct pathways have been found of ACC-core UCDW onto the Palmer Deep Canyon, so no ACC-core UCDW is present in the canyon, but by looking at T_{\max} at depth, we find a modified-UCDW (relatively colder and fresher than pure UCDW) at depth. Because the bulk of the mUCDW is found at deeper depths and the gliders are usually only sampling the upper 100 m of the water column, we are only partially capturing this intrusion onto the canyon. This intrusion however is not observed to reach the euphotic zone until after the growing season. Therefore it is unlikely that it plays an important role in supplying nutrients to primary producers over the canyon during the growing season.

The WW, identified by T_{\min} in the profile, was found above mUCDW. This water mass is the remnant surface water from the preceding winter season and is typically found at 50–60 m. WW has a very clear seasonal pattern (Figure 5), showing a well-defined and strong presence early in the season, followed by erosion by mixing with warmer water from above and below as the season progresses. The increase in solar radiation and winds, typical of the late summer season in the region, deepens the MLD, further mixing AASW with the WW below. As the latter, saltier water mass is slowly eroded, together with the decrease in freshwater input later in the season due to the reduction in sea ice meltwater, a marked increase in the overall salinity of surface water is observed.

4.1.2. Phytoplankton Seasonal Dynamics

In the WAP, chlorophyll-*a* variability has been correlated with local physical forcing such as wind, water column stability, and sea ice [Saba *et al.*, 2014]. The relationship between sea ice dynamics and biological productivity is complex. While decreasing sea ice cover can remove the shading effect of ice resulting in higher productivity, as seen in the southern region of the WAP [Montes-Hugo *et al.*, 2009; Saba *et al.*, 2014], at the same time, the decrease in fresh water input from melting sea ice will result in lower stratification and likely deeper MLDs, which should lead to decreased primary production resulting from decreasing average light levels [Vernet *et al.*, 2008].

The high variability in the timing of the sea ice retreat [Stammerjohn *et al.*, 2008] matches the high variability seen in the MLD (*y*-axis, Figure 3) in late December. Shallower MLDs in the early growing season show both increased stability (Figure 4) and decreased salinity (Figure 3d). They have been associated with low wind speeds over weekly timescales [Moline, 1998; Moline and Prezelin, 1996], freshwater input from glacial and sea ice melt [Meredith *et al.*, 2008], and surface warming from incoming solar energy. The input of fresh water from glacial and sea ice melting shoals the MLD, increases the stability of the water column [Garibotti *et al.*, 2003] and restricts deep mixing. This creates a stable upper water column in which phytoplankton cells are allowed to remain in a favorable light regime [Garibotti *et al.*, 2003; Vernet *et al.*, 2008]. In addition, the canyon's proximity to land shelters the canyon head from storms and strong winds seen offshore [Hofmann *et al.*, 1996], helping to maintain the observed shallow and stable MLD. Modeling work by Mitchell and Holm-Hansen [1991] concluded that intense phytoplankton blooms develop when MLD is shallower than 25 m, there is no limitation by nutrients and specific loss rate is $\sim 0.3\text{--}0.35\text{ d}^{-1}$, with grazing and respiration comprising over 2/3 of this loss. Although we do not have direct measurements of nutrients or loss rates at the same time as the glider profiles, our MLD and chlorophyll data match this model, with high concentrations of chlorophyll observed in MLD of 25–30 m or shallower and declining when the MLD is deeper. Note that there was a decrease in ML-averaged chlorophyll when MLD shoals to values close to 10 m (Figure 7), suggesting some photoinhibition processes due to high light or light limitation by self-shading [Moline *et al.*, 1996].

The mechanisms driving the chlorophyll decrease later in the growing season remain an open question. Data show that decreases in ML-averaged chl-*a* are accompanied by a deepening of the ML (Figures 3

and 7). Decrease in freshwater input together with increased vertical mixing from wind forcing causes MLD to deepen and water stability to decrease. Another contributor to this decreased water column stability is the warming of WW by vertical mixing with intruding mUCDW from below. The deepening of the ML can decrease the ML-averaged chl-*a* concentrations by diluting a high concentration of phytoplankton over a larger depth interval; this idea is also supported by the increase in ML-integrated chl-*a* as MLD deepens (red line; Figure 7a), indicating there are phytoplankton below the MLD. While the deepening of the ML alone could drive down the ML-averaged chl-*a* concentrations as it also decreases the mean light levels required for phytoplankton photosynthesis [Mitchell and Holm-Hansen, 1991], other factors, such as nutrient limitation and grazing, can also play a role in this decrease. Although gliders do not provide in situ measurements of the nutrient concentrations in the water column, an inspection of historical nutrient data from the LTER Station E (6.5 km NE of the sampled area) shows that no macronutrient limitation is observed throughout the season [Ducklow *et al.*, 2012]. The scarce micronutrient (trace metal) studies in the region make it difficult to evaluate the micronutrient limitation question, especially regarding iron deficiency after a bloom. Iron is known to be a limiting factor controlling primary productivity in the Southern Ocean, mainly due to the lack of efficient supply mechanisms [Boyd *et al.*, 2012]. However, recent studies have shown that regions in close proximity to the coast in Antarctica, such as canyon heads, are not iron limited, and that in certain parts of the WAP there is enough iron to allow the potential utilization of all macronutrients available [Annett *et al.*, 2015]. Surface dissolved Fe:PO₄ ratios measured at Station E were always above 1.1 mmol mol⁻¹, much higher than cellular Fe:P~0.2 mmol mol⁻¹ measured in Fe-limited Southern Ocean waters [Twining and Baines, 2013]. In addition, dissolved Fe was always >0.5 nmol/kg (Figure 3), higher than dissolved Fe concentrations ~0.1 nmol kg⁻¹ typical of Fe-limited waters [Sedwick *et al.*, 2008], further supporting our inference that Fe is not limiting phytoplankton production at the head of Palmer Canyon. Increases in surface dissolved Fe concentrations at Station E (Figure 3) are concurrent with the deepening of the ML, indicating a potential source of iron to the surface waters. The presence of WW, acting as a physical barrier between the AASW and mUCDW implies that this Fe source is likely related to vertical mixing from shallow sediments or lateral advection of surface inputs such as glacial meltwater. Losses by grazing are likely a contributing cause of chl-*a* decline as canyons are known to aggregate zooplankton prey for the apex predators [Bernard and Steinberg, 2013], however, we do not have concurrent zooplankton data to address this question.

The timing of a secondary shoaling of the MLD in late February/early March is matched with a freshening of the ML and a small increase in water column stability. The rising air temperatures in the summer months drive the increased fresh, glacial meltwater input onto the surface coastal waters. Concurrent with this, a secondary peak in chl-*a* is observed, consistent with previous work by Moline and Prezelin [1996], and a reduction of dissolved Fe to intermediate values, presumably a result of decreased supply from below and increased Fe removal in association with the chl-*a* increase, balancing the increased supply of Fe from glacial meltwater.

4.2. Palmer Deep Cross-Canyon Spatial Analysis

While most phytoplankton studies in the WAP canyons have focused on the temporal (seasonal and inter-annual) variability [Kavanaugh *et al.*, 2015; Moline and Prezelin, 1996], little is known about what is driving the high small-scale spatial variability observed in the foraging behavior of penguins [Oliver *et al.*, 2013]. Spatial differences in phytoplankton are also likely to occur as a cyclonic eddy feature is expected to dominate the upper water column circulation over the canyon and to aggregate small nonmigratory species at the head of canyons, particularly at the downstream side of the canyon [Allen *et al.*, 2001].

Preliminary analysis of CODAR High-Frequency Radar (HFR) data at PD [Kohut *et al.*, 2014], which provides surface maps of ocean currents, shows on average for the months of January and February, a strong North-eastward (onshore) current toward the Bismarck Strait that crosses the southern region of this study, with average speeds an order of magnitude faster than the flow that crosses the northern region. On the other hand, although a less prominent feature, a weaker Southeastward (offshore) coastal current crosses the northern flank of the transect. Initial analysis of the mean current standard deviation shows higher variability in the flow that crosses the southern region [Todoroff *et al.*, 2015]. This highly energetic and variable flow can explain the increased variability in the water properties in that region as seen in Figures 5 and 6. This variability decreases with the temporal evolution of the water masses, with surface water becoming warmer and saltier and with WW being warmed both from above and below. Main spatial differences in

water properties can be found at depth, with the northern region showing overall colder temperatures, as evident by the presence of WW until later in the season. The southern flank shows intrusions of warm, salty, deep water likely from the onshore current forcing mUCDW onto the shelf that then mixes upward, weakening the signal of WW from below (Figure 8). The northern flank shows a strong presence of winter water and a fresh water lens that comes from glacial and sea ice melt brought by the coastal current. The differences in magnitude and the variability of the currents between the two regions are likely to contribute to the stability of the MLD dynamics on local scales. With less energetic currents, the water in the northern region is likely to show higher residence times, ideal for local primary production to occur. On the other hand, southern region mean currents show higher variability and magnitude that can potentially impede local production to fully thrive as the timescales of the mean currents are shorter than the doubling time of Antarctic phytoplankton.

Another factor known to control primary production is the availability of iron [Twining and Baines, 2013]. Although there are several potential sources of iron to surface waters (glacial melt, sea-ice melt, seawater interaction with shallow sediments, atmospheric input and deep water upwelling), glacial meltwater has been identified as one of the most important [Dierssen *et al.*, 2002; Hawkings *et al.*, 2014], by its volume flux and because of the continuous yet variable supply during the growing season [Meredith *et al.*, 2008]. The close proximity of canyon head systems on the WAP to the coast where glaciers are prominent features, may also contribute favorably to the increased production seen in the canyon as the increased glacial meltwater input (and pushed by the coastal current) contributes to increased water column stability and is a potential source of iron to the system [Alderkamp *et al.*, 2015; Annett *et al.*, 2015; Arrigo *et al.*, 2015]. While mUCDW upwelling enriched with iron from sediments has been proposed as a potential source of iron to coastal WAP regions [Annett *et al.*, 2015], at Ryder Bay (340 km south of Palmer Deep) it was found to account for very little of the iron input due to the highly stratified waters during the growth season. It is however identified as an important source of iron over annual or longer time-scales. The same seems true for the overall nutrient budget. Glider observations during the austral spring and summer show no evidence of this mUCDW upwelling reaching surface waters during the growth season as there is a clear layer of WW physically separating surface waters from the deep waters below while the bloom is present. However, this water mass is slowly warming throughout the season due to vertical mixing from above and below, contributing to the decreased water column stability. While there is no evidence of the surface waters at PD being limited by macro or micronutrients at any point, a drawdown in the nutrient pool is apparent while the bloom is thriving [Ducklow *et al.*, 2012]. After the growth season, as the stratification weakens, mUCDW intrusions from below will replenish the surface water with both micro and macronutrients required for the following year's spring phytoplankton bloom.

5. Conclusions

Understanding the spatial and temporal variability of phytoplankton is important, especially to assess the dynamics of higher trophic levels as they are dependent on primary producers for food source. The high-resolution capabilities of gliders allow sampling and coverage at appropriate scales to evaluate phytoplankton dynamics. Using the 6 year glider observations over PD, we were able to describe the fine temporal and spatial variability of the phytoplankton seasonal cycle and relate it to its main physical drivers, namely MLD and water stability. Although interannual variability was observed in the data, the shoaling of the MLD in late spring matching increased chlorophyll concentration was a pattern observed in all years sampled (2010–2015), as more light becomes available to the phytoplankton community. Following this period, a summer (February) deepening of the MLD was accompanied by decreased chlorophyll concentration.

Observations showed that MLD dynamics and chlorophyll variability were tightly coupled in both time and space. Spatial variability was evaluated by glider transects across the head of the canyon. While MLD dynamics was similar in the northern and southern canyon regions, the physical setting observed in different regions of the canyon, such as water column stratification and water masses present, explain some of the observed chlorophyll variability. Preliminary analysis of surface currents provides an insight on what could be driving some of the observed differences in water column structure that are key for phytoplankton development. The northern region with increased chlorophyll showed a more coastal influence, with increased freshwater input, slower currents, and increased stratification, while the southern region with

lower chlorophyll showed more influence from offshore with faster currents and more intrusions of mUCDW from below. However, further sampling and analysis is necessary to evaluate whether water column physics is driving the spatial differences in chlorophyll concentrations alone or if iron supply plays a role in the system at any point in the growth season.

Acknowledgments

We thank the two anonymous reviewers whose suggestions helped improve and clarify this manuscript. The research was supported by the National Science Foundation grants ANT-0823101 (Palmer-LTER), ANT-1327248 and ANT-1326541 (CONVERGE) and ANT-1142250 (iron WAP). Filipa Carvalho was funded by a Portuguese doctoral fellowship from Fundação para a Ciência e Tecnologia (DFRH-SFRH/BD/72705/2010). Glider data can be accessed at ERDDAP server at <http://erddap.marine.rutgers.edu/erddap/info/>. Weather data can be accessed at <http://oceaninformatics.ucsd.edu/datazoo/data/pallter/datasets>.

References

- Alderkamp, A., G. L. van Dijken, K. E. Lowry, T. L. Connelly, M. Lagerström, R. M. Sherrell, C. Haskins, E. Rogalsky, O. Schofield, and S. E. Stammerjohn (2015), Fe availability drives phytoplankton photosynthesis rates during spring bloom in the Amundsen Sea Polynya, Antarctica, *Elementa*, 3(1), 000043.
- Allen, S. E., and X. D. de Madron (2009), A review of the role of submarine canyons in deep-ocean exchange with the shelf, *Ocean Sci.*, 5(4), 607–620.
- Allen, S. E., C. Vindeirinho, R. E. Thomson, M. G. G. Foreman, and D. L. Mackas (2001), Physical and biological processes over a submarine canyon during an upwelling event, *Can. J. Fish. Aquat. Sci.*, 58(4), 671–684, doi:10.1139/cjfas-58-4-671.
- Annett, A. L., M. Skiba, S. F. Henley, H. J. Venables, M. P. Meredith, P. J. Statham, and R. S. Ganeshram (2015), Comparative roles of upwelling and glacial iron sources in Ryder Bay, coastal western Antarctic Peninsula, *Mar. Chem.*, 176, 21–33, doi:10.1016/j.marchem.2015.06.017.
- Arrigo, K. R., G. L. van Dijken, and A. L. Strong (2015), Environmental controls of marine productivity hot spots around Antarctica, *J. Geophys. Res. Oceans*, 120, 5545–5565, doi:10.1002/2015JC010888.
- Behrenfeld, M. J., E. Boss, D. A. Siegel, and D. M. Shea (2005), Carbon-based ocean productivity and phytoplankton physiology from space, *Global Biogeochem. Cycles*, 19, GB1006, doi:10.1029/2004GB002299.
- Bernard, K. S., and D. K. Steinberg (2013), Krill biomass and aggregation structure in relation to tidal cycle in a penguin foraging region off the Western Antarctic Peninsula, *ICES J. Mar. Sci.*, 70(4), 834–849, doi:10.1093/icesjms/fst088.
- Boyd, P. W., K. R. Arrigo, R. Strzepek, and G. L. van Dijken (2012), Mapping phytoplankton iron utilization: Insights into Southern Ocean supply mechanisms, *J. Geophys. Res.*, 117, C06009, doi:10.1029/2011JC007726.
- Bruno, M., A. Vazquez, J. Gomez-Enri, J. M. Vargas, J. G. Lafuente, A. Ruiz-Canavate, L. Mariscal, and J. Vidal (2006), Observations of internal waves and associated mixing phenomena in the Portimao Canyon area, *Deep Sea Res., Part II*, 53(11–13), 1219–1240, doi:10.1016/j.dsr2.2006.04.015.
- Chu, P. C., and C. W. Fan (2011), Maximum angle method for determining mixed layer depth from seaglider data, *J. Oceanogr.*, 67(2), 219–230, doi:10.1007/s10872-011-0019-2.
- Clarke, A., M. P. Meredith, M. I. Wallace, M. A. Brandon, and D. N. Thomas (2008), Seasonal and interannual variability in temperature, chlorophyll and macronutrients in northern Marguerite Bay, Antarctica, *Deep Sea Res., Part II*, 55(18–19), 1988–2006, doi:10.1016/j.dsr2.2008.04.035.
- Dierssen, H. M., R. C. Smith, and M. Vernet (2002), Glacial meltwater dynamics in coastal waters west of the Antarctic peninsula, *Proc. Natl. Acad. Sci. U. S. A.*, 99(4), 1790–1795, doi:10.1073/pnas.032206999.
- Ducklow, H. W., K. Baker, D. G. Martinson, L. B. Quetin, R. M. Ross, R. C. Smith, S. E. Stammerjohn, M. Vernet, and W. Fraser (2007), Marine pelagic ecosystems: The west Antarctic Peninsula, *Philos. Trans. R. Soc. B*, 362(1477), 67–94.
- Ducklow, H. W., A. Clarke, R. Dickhut, S. C. Doney, H. Geisz, K. Huang, D. G. Martinson, M. P. Meredith, H. V. Moeller, and M. Montes-Hugo (2012), The Marine System of the Western Antarctic Peninsula, in *Antarctic Ecosystems: An Extreme Environment in a Changing World*, edited by A. D. Rogers, et al., pp. 121–159, John Wiley & Sons, Ltd., Chichester, U. K., doi:10.1002/9781444347241.ch5.
- Erdmann, E. S., C. A. Ribic, D. L. Patterson-Fraser, and W. R. Fraser (2011), Characterization of winter foraging locations of Adélie penguins along the Western Antarctic Peninsula, 2001–2002, *Deep Sea Res., Part II*, 58(13–16), 1710–1718, doi:10.1016/j.dsr2.2010.10.054.
- Fragoso, G. M., and W. O. Smith (2012), Influence of hydrography on phytoplankton distribution in the Amundsen and Ross Seas, Antarctica, *J. Mar. Syst.*, 89(1), 19–29, doi:10.1016/j.jmarsys.2011.07.008.
- Fraser, W. R., and W. Z. Trivelpiece (1996), Factors controlling the distribution of seabirds: Winter-summer heterogeneity in the distribution of Adélie penguin populations, *Antarct. Res. Ser.*, 70, 257–272.
- Garibotti, I. A., M. Vernet, M. E. Ferrario, R. C. Smith, R. M. Ross, and L. B. Quetin (2003), Phytoplankton spatial distribution patterns along the western Antarctic Peninsula (Southern Ocean), *Mar. Ecol. Prog. Ser.*, 261, 21–39, doi:10.3354/meps261021.
- Harris, P. T., and T. Whiteway (2011), Global distribution of large submarine canyons: Geomorphic differences between active and passive continental margins, *Mar. Geol.*, 285(1–4), 69–86, doi:10.1016/j.margeo.2011.05.008.
- Hawkings, J. R., J. L. Wadham, M. Tranter, R. Raiswell, L. G. Benning, P. J. Statham, A. Tedstone, P. Nienow, K. Lee, and J. Telling (2014), Ice sheets as a significant source of highly reactive nanoparticulate iron to the oceans, *Nat. Commun.*, 5, 3929, doi:10.1038/ncomms4929.
- Helbling, E. W., V. Villafane, and O. Holm-Hansen (1991), Effect of Iron on Productivity and Size Distribution of Antarctic Phytoplankton, *Limnol. Oceanogr.*, 36(8), 1879–1885.
- Hofmann, E. E., J. M. Klinck, C. M. Lascara, and D. A. Smith (1996), Water mass distribution and circulation west of the Antarctic Peninsula and including Bransfield Strait, in *Foundations for Ecological Research West of the Antarctic Peninsula*, edited by R. M. Ross, E. E. Hofmann and L. B. Quetin, AGU, Washington, D. C., doi:10.1029/AR070p0061.
- Holm-Hansen, O., and B. Mitchell (1991), Spatial and temporal distribution of phytoplankton and primary production in the western Bransfield Strait region, *Deep Sea Res. Part A*, 38(8), 961–980.
- Kahl, L. A., O. Schofield, and W. R. Fraser (2010), Autonomous gliders reveal features of the water column associated with foraging by Adélie penguins, *Integr. Comp. Biol.*, 50(6), 1041–1050, doi:10.1093/icb/icq098.
- Kavanaugh, M. T., F. N. Abdala, H. Ducklow, D. Glover, W. Fraser, D. Martinson, S. Stammerjohn, O. Schofield, and S. C. Doney (2015), Effect of continental shelf canyons on phytoplankton biomass and community composition along the western Antarctic Peninsula, *Mar. Ecol. Prog. Ser.*, 524, 11–26, doi:10.3354/meps11189.
- Kohut, J., E. Hunter, and B. Huber (2013), Small-scale variability of the cross-shelf flow over the outer shelf of the Ross Sea, *J. Geophys. Res. Oceans*, 118, 1863–1876, doi:10.1002/jgrc.20090.
- Kohut, J., K. Bernard, W. Fraser, M. J. Oliver, H. Statscevvich, P. Winsor, and T. Miles (2014), Studying the impacts of local oceanographic processes on Adélie penguin foraging ecology, *Mar. Technol. Soc. J.*, 48(5), 25–34.
- Kunze, E., L. K. Rosenfeld, G. S. Carter, and M. C. Gregg (2002), Internal waves in Monterey Submarine Canyon, *J. Phys. Oceanogr.*, 32(6), 1890–1913, doi:10.1175/1520-0485(2002)032<1890:WIMSC>2.0.CO;2.

- Lagerström, M., M. Field, M. Séguret, L. Fischer, S. Hann, and R. Sherrell (2013), Automated on-line flow-injection ICP-MS determination of trace metals (Mn, Fe, Co, Ni, Cu and Zn) in open ocean seawater: Application to the GEOTRACES program, *Mar. Chem.*, *155*, 71–80.
- Lorbacher, K., D. Dommenges, P. P. Niiler, and A. Köhl (2006), Ocean mixed layer depth: A subsurface proxy of ocean-atmosphere variability, *J. Geophys. Res.*, *111*, C07010, doi:10.1029/2003JC002157.
- Martin, J. H., S. E. Fitzwater, and R. M. Gordon (1990), Iron deficiency limits phytoplankton growth in Antarctic waters, *Global Biogeochem. Cycles*, *4*(1), 5–12.
- Martinson, D. G., and D. C. McKee (2012), Transport of warm upper circumpolar deep water onto the western Antarctic Peninsula continental shelf, *Ocean Sci.*, *8*(4), 433–442, doi:10.5194/os-8-433-2012.
- Martinson, D. G., S. E. Stammerjohn, R. A. Iannuzzi, R. C. Smith, and M. Vernet (2008), Western Antarctic Peninsula physical oceanography and spatio-temporal variability, *Deep Sea Res., Part II*, *55*(18–19), 1964–1987, doi:10.1016/j.dsr2.2008.04.038.
- Meredith, M. P., M. A. Brandon, M. I. Wallace, A. Clarke, M. J. Leng, I. A. Renfrew, N. P. Van Lipzig, and J. C. King (2008), Variability in the freshwater balance of northern Marguerite Bay, Antarctic Peninsula: Results from hwater b, *Deep Sea Res., Part II*, *55*(3), 309–322.
- Mitchell, B. G., and O. Holm-Hansen (1991), Observations of modeling of the Antarctic phytoplankton crop in relation to mixing depth, *Deep Sea Res., Part A*, *38*(8), 981–1007.
- Moline, M. A. (1998), Photoadaptive response during the development of a coastal Antarctic diatom bloom and relationship to water column stability, *Limnol. Oceanogr.*, *43*(1), 146–153.
- Moline, M. A., and B. B. Prezelin (1996), Long-term monitoring and analyses of physical factors regulating variability in coastal Antarctic phytoplankton biomass, in situ productivity and taxonomic composition over subseasonal, seasonal and interannual time scales, *Mar. Ecol. Prog. Ser.*, *145*(1–3), 143–160, doi:10.3354/meps145143.
- Moline, M. A., B. B. Prezelin, and H. Claustre (1996), Light-saturated primary production in antarctic coastal waters, *Antarct. J. U. S.*, *31*(5), 105–107.
- Moline, M. A., B. B. Prezelin, O. Schofield, and R. C. Smith (1997), Temporal dynamics of coastal Antarctic phytoplankton: Environmental driving forces and impact of 1991/92 summer diatom bloom on the nutrient regimes, in *Antarctic Communities: Species, Structure and Survival*, edited by B. Battaglia, J. Valencia, and D. W. H. Walton, pp. 67–72, Cambridge Univ. Press, Cambridge.
- Montes-Hugo, M. A., M. Vernet, D. Martinson, R. Smith, and R. Iannuzzi (2008), Variability on phytoplankton size structure in the western Antarctic Peninsula (1997–2006), *Deep Sea Res., Part II*, *55*(18–19), 2106–2117, doi:10.1016/j.dsr2.2008.04.036.
- Montes-Hugo, M. A., S. C. Doney, H. W. Ducklow, W. Fraser, D. Martinson, S. E. Stammerjohn, and O. Schofield (2009), Recent changes in phytoplankton communities associated with rapid regional climate change along the western Antarctic Peninsula, *Science*, *323*(5920), 1470–1473, doi:10.1126/science.1164533.
- Montes-Hugo, M. A., C. Sweeney, S. C. Doney, H. Ducklow, R. Frouin, D. G. Martinson, S. Stammerjohn, and O. Schofield (2010), Seasonal forcing of summer dissolved inorganic carbon and chlorophyll a on the western shelf of the Antarctic Peninsula, *J. Geophys. Res.*, *115*, C03024, doi:10.1029/2009JC005267.
- Nelson, D. M., and W. Smith (1991), The role of light and major nutrients, *Limnol. Oceanogr.*, *36*, 1650–1661.
- Oliver, M. J., M. A. Moline, I. Robbins, W. Fraser, D. Patterson, and O. Schofield (2012), Letting penguins lead: Dynamic modeling of penguin locations guides autonomous robotic sampling, *Oceanography*, *25*(3), 120–121.
- Oliver, M. J., A. Irwin, M. A. Moline, W. Fraser, D. Patterson, O. Schofield, and J. Kohut (2013), Adelie penguin foraging location predicted by tidal regime switching, *PLoS One*, *8*(1), e55163, doi:10.1371/journal.pone.0055163.
- Prézelin, B. B., E. E. Hofmann, C. Mengelt, and J. M. Klinck (2000), The linkage between Upper Circumpolar Deep Water (UCDW) and phytoplankton assemblages on the west Antarctic Peninsula continental shelf, *J. Mar. Res.*, *58*(2), 165–202.
- Prézelin, B. B., E. E. Hofmann, M. Moline, and J. M. Klinck (2004), Physical forcing of phytoplankton community structure and primary production in continental shelf waters of the Western Antarctic Peninsula, *J. Mar. Res.*, *62*(3), 419–460.
- Saba, G. K., et al. (2014), Winter and spring controls on the summer food web of the coastal West Antarctic Peninsula, *Nat. Commun.*, *5*, 4318, doi:10.1038/ncomms5318.
- Sakshaug, E., G. Johnsen, K. Andresen, and M. Vernet (1991), Modeling of light-dependent algal photosynthesis and growth: Experiments with the Barents sea diatoms *Thalassiosira nordenskiöldii* and *Chaetoceros furcellatus*, *Deep Sea Res., Part A*, *38*(4), 415–430.
- Schofield, O., et al. (2007), Slocum gliders: Robust and ready, *J. Field Robot.*, *24*(6), 473–485, doi:10.1002/rob.20200.
- Schofield, O., H. W. Ducklow, D. G. Martinson, M. P. Meredith, M. A. Moline, and W. R. Fraser (2010), How do polar marine ecosystems respond to rapid climate change?, *Science*, *328*(5985), 1520–1523.
- Schofield, O., et al. (2013), Penguin biogeography along the west antarctic peninsula testing the canyon hypothesis with Palmer LTER observations, *Oceanography*, *26*(3), 204–206.
- Sedwick, P. N., A. R. Bowie, and T. W. Trull (2008), Dissolved iron in the Australian sector of the Southern Ocean (CLIVAR SR3 section): Meridional and seasonal trends, *Deep Sea Res., Part I*, *55*(8), 911–925, doi:10.1016/j.dsr.2008.03.011.
- Serebrennikova, Y. M., and K. A. Fanning (2004), Nutrients in the Southern Ocean GLOBEC region: Variations, water circulation, and cycling, *Deep Sea Res., Part II*, *51*(17–19), 1981–2002, doi:10.1016/j.dsr2.2004.07.023.
- Smith, R. C., K. S. Baker, and M. Vernet (1998), Seasonal and interannual variability of phytoplankton biomass west of the Antarctic Peninsula, *J. Mar. Syst.*, *17*(1–4), 229–243, doi:10.1016/S0924-7963(98)00040-2.
- Smith, R. C., D. G. Martinson, S. E. Stammerjohn, R. A. Iannuzzi, and K. Ireson (2008), Bellingshausen and western Antarctic Peninsula region: Pigment biomass and sea-ice spatial/temporal distributions and interannual variability, *Deep Sea Res., Part II*, *55*(18–19), 1949–1963, doi:10.1016/j.dsr2.2008.04.027.
- Stammerjohn, S. E., D. G. Martinson, R. C. Smith, and R. A. Iannuzzi (2008), Sea ice in the western Antarctic Peninsula region: Spatiotemporal variability from ecological and climate change perspectives, *Deep Sea Res., Part II*, *55*(18–19), 2041–2058, doi:10.1016/j.dsr2.2008.04.026.
- Todoroff, K., J. Kohut, P. Winsor, and H. Statscewich (2015), Spatial circulation patterns over Palmer Deep canyon and the effects on Adélie Penguin foraging, paper presented at OCEANS 2015-MTS/IEEE Washington, IEEE, Washington, D. C., 19–22 Oct.
- Twining, B. S., and S. B. Baines (2013), The trace metal composition of marine phytoplankton, *Ann. Rev. Mar. Sci.*, *5*, 191–215, doi:10.1146/annurev-marine-121211-172322.
- Vernet, M., D. Martinson, R. Iannuzzi, S. Stammerjohn, W. Kozlowski, K. Sines, R. Smith, and I. Garibotti (2008), Primary production within the sea-ice zone west of the Antarctic Peninsula: I-Sea ice, summer mixed layer, and irradiance, *Deep Sea Res., Part II*, *55*(18–19), 2068–2085, doi:10.1016/j.dsr2.2008.05.021.